The Influence of Polyvinylidene Fluoride (PVDF) Binder Properties on $LiNi_{0.33}Co_{0.33}Mn_{0.33}O_2$ (NMC) Electrodes Made by a Dry-Powder-Coating Process

Ming Wang, *,z **Jiazhi Hu,** * **Yikai Wang,** * **and Yang-Tse Cheng**

Department of Chemical and Materials Engineering, University of Kentucky, Lexington, Kentucky 40506, USA

We have investigated the effects of the molecular weight of the polyvinylidene fluoride (PVDF) binder on the electrochemical performance and mechanical integrity of the $LiNi_{0.33}Co_{0.33}Mn_{0.33}O_2$ (NMC) electrodes made by a dry-powder-coating process. The microstructure, binding strength, and electrochemical behavior of the electrodes made with two types of PVDF polymers were compared. We show that a thin PVDF layer can form on the NMC particle surface after heating the PVDF to above its melting point. The microstructure and porosity of the PVDF layer depend strongly on the molecular weight of the PVDFs. With increasing molecular weight, the PVDF layer becomes more porous, improving the high-rate capacity without decreasing binding strength and long-term cycling performance of the electrodes.

© The Author(s) 2019. Published by ECS. This is an open access article distributed under the terms of the Creative Commons Attribution 4.0 License (CC BY, http://creativecommons.org/licenses/by/4.0/), which permits unrestricted reuse of the work in any medium, provided the original work is properly cited. [DOI: 10.1149/2.1171910jes]

Manuscript submitted April 29, 2019; revised manuscript received May 29, 2019. Published June 21, 2019.

Rechargeable lithium-ion batteries (LIBs) are broadly used in our daily lives because of their relatively high energy density and power density.[1,2] However, LIBs are expansive for many applications.[3,4] Today, a typical electrode fabrication starts with mixing active materials, conductive agents, polymeric binders, and solvents to form a slurry, casting the slurry onto metal foil (Al or Cu) when it reaches appropriate viscosity, drying the slurry to form the porous electrode.[5] The dried electrodes are calendared to improve electrical conductivity and further dried to remove the residual solvent and moisture before making the cells.[6] Many commercial LIBs use polyvinylidene fluoride (PVDF) as the binder because of its excellent electrochemical stability, wettability with the electrolytes, and acceptable adhesion strength between electrode laminates and current collectors.[7] PVDF is a synthetic polymer with long-chain, semi-crystalline structure with the repeat unit (CH_2CF_2), which requires N-Methyl-2-pyrrolidone (NMP) as the solvent to dissolve the polymer particles to make the slurry. The usage of NMP increases the material and manufacturing cost of the electrode because NMP is expensive, toxic, and flammable, as well as requiring energy to dry and capture.[4,6,8–15] By eliminating the usage of NMP, the cost of electrode fabrication could be reduced by about 15%.[16]

Electrostatic spray deposition (ESD), a dry powder coating process, is one of the promising methods to reduce the production cost of LIBs by eliminating the usage of organic solvents.[16–18] ESD is commonly used in automotive painting, food, and pharmaceutical processing.[19] For battery manufacturing research, ESD has been used to make electrodes with designed morphologies.[20] During the ESD process, the particles are charged by a high voltage. After the charged particles are deposited on the grounded metal substrate, each particle induces a charge with equal value but opposite polarity (mirror charge) on the grounded metal surface. The opposite charges provide the electrostatic force to hold the particles to the metal surface.

A few research groups have explored the ESD process to make electrodes. Hiroya et al. reported a cathode fabrication process using a tribo-charging gun.[18] The dry-mixed electrode powders contain $LiCoO_2$ (LCO, active material), carbon nanoparticles (conductive additive) and the polymethyl methacrylate nanoparticles (PMMA, polymeric binder) were sprayed into air to form charged powder cloud. The charged powders were transferred to a grounded aluminum substrate and rolled into electrodes. Ludwig et al. reported the fabrication of electrodes containing LCO or $LiNi_{0.33}Co_{0.33}Mn_{0.33}O_2$ (NMC), carbon black and PVDF using ESD and hot-rolling to improve the electrode binding strength.[16] Al-Shroofy et al. reported the fabrication method of NMC electrodes using ESD, oven baking and room temperature-rolling.[17] The electrodes were reported to have a capacity retention of 80% for more than 300 cycles. Liu et al. reported the fabrication of long-life electrodes containing a 90 wt% NMC with ESD and hot-rolling, which have capacity retention of more than 80% after 500 cycling.[21]

For the conventional wet-slurry-coating process, the PVDF polymers are dissolved in NMP solvent, and the polymer chains disentangle to random coil structure.[22] According to Zheng et al., the active particles in the electrode slurry are surrounded by PVDF chains after mixing.[23] The PVDF polymers with high molecular weight are selected as the binders to prevent agglomeration or sedimentation during slurry casting and drying processes.[24] Although the influence of PVDF properties on the wet-slurry-coated electrodes has been investigated extensively,[24–27] their effects on dry-coated electrodes are still unknown. Thus, it is important to investigate how the PVDF properties affect the electrodes made by the ESD process.

By conducting microstructure observations, peel strength tests, scratch tests, and electrochemical measurements, we uncover, in this paper, the influence of the molecular weight of PVDFs on the NMC electrodes made by ESD.

Experimental

Properties of PVDF binders.—Two commercially available PVDF polymers of different molecular weight were used as electrode binders, one from Arkema (Kynar HSV 900, labeled as "HSV 900") and another from Alfa Aesar (Alfa Aesar 44080, labeled as "Alfa Aesar"). Several properties of the PVDF polymers are collected in Table I.[28–31] The particle size of the powders was determined from Scanning Electron Microscope (SEM) images, shown in Fig. S1 in the supplementary information.

Electrode fabrication.—*Preparation of electrode powders.*—The powder mixtures, composed of 90 wt% $LiNi_{0.33}Co_{0.33}Mn_{0.33}O_2$ (NMC, Umicore), 5 wt% conductive carbon black (CB, TIMCAL Super C65), and 5 wt% PVDF, were prepared in a planetary mixer (Mazerustar KK-250S, Kurabo) for 4 cycles. Each cycle was 4 minutes in duration (revolution speed level 3, rotation speed level 9). The temperature of the powders at the end of the mixing cycle was less than 70°C, measured by an infrared thermometer (ETEKCITY). The powder mixture was cooled in air between each cycle for approximately 1 minute.

Preparation of electrodes.—A manually operated powder coating spray gun (Encore LT Manual Powder Coating System, Nordson) was used for the ESD process. One piece of 16 μm thick aluminum foil was used as the electrode substrate, one piece of electrically grounded Cu plate (250 μm thick) was used as the platform. The operation voltage was 25 kV. Both atomizing and flow pressures were 7 psi. The spraying

*Electrochemical Society Member.
zE-mail: ming.wang@uky.edu

MRD EX. 2013
LGES v MRD
IPR2024-01013

Table I. Properties of the two types of PVDF polymers used in this study.[1–3]

PVDF	Particle size (μm)	Melting temperature (°C)	Molecular weight (kDa)	Melt viscosity at 230°C, 100 rad s^{-1} (kPoise)	Melt flow rate at 230°C, 21.6 kg load (g per 10 min)	Specific gravity (g cm^{-3})
HSV 900	2-40	162-172	92840 and 1367	47-53	N/A	1.78
Alfa Aesar	6-50	155-160	350	24-30	6-14	1.76

time was 45 seconds. The spray direction was 45° with a 20 cm distance between the spray gun tip and the aluminum substrate. The thermal activation was done by transferring the dry-powder-coated electrodes to an oven (DKN812, Yamato) and baking in air. Different baking durations and temperatures were used as the thermal activation process and baking at 200°C for 1 hour was selected for the optimal results.

The baked electrodes were calendered at room temperature with a 10 μm gap spacing by a compact electrical rolling press (MTI Corp.). The calendered electrodes were punched into 12 mm diameter discs by a precision disc cutter (MTI corp.) and transferred to a glove box. The porosity of the dry-coated electrodes was about 30% after calendering. The average loading of the electrode discs was 2.4 mAh/cm^2. The average thickness after calendering was 59 μm.

Characterization.—*Morphology characterization.*—The surface morphology was investigated using a Scanning Electron Microscope (SEM) with Energy Dispersive Spectroscopy (EDS) (FEG 250, Quanta).

Mechanical measurements.—The binding strength of the dry-powder-coated electrodes was measured by peel test and scratch test. The binding strength was measured by a 180° peel test (MH2-110, Imada, Inc.) based on the ASTM-D903 standard. The speed was 60 mm per min. The Al foil was cut into 1 cm width strips ahead of the dry-powder-coating process. The coated strips were heated at 200°C in an oven and calendered individually. The calendered strip was attached to the sample stage by a double-sided adhesive tape. The cohesive strength between NMC particles was measured by a scratch test (NanoTest Vantage, Micro Materials Limited) using a conical diamond stylus. The tip radius was 10 μm, and the cone angle was 60°. A 12 mm diameter electrode disc was glued to a flat sample stage as the scratch sample. A 2000 μm scratch was made by sliding the sample against the tip. The applied load was from 0.1 mN to 20 mN.

Coin cell fabrication and electrochemical measurements.—The coin cells (CR2025) were assembled using an automatic coin cell crimper (KTE-20S-D, Hohsen) inside an argon-filled glove box (MBraun). A lithium metal foil (99.9%, Sigmae-Aldrich) was used as the counter electrode. One piece of polypropylene membrane (Celgard 2400) was used as the separator. The electrolyte was 1 M LiPF6 in ethylene carbonate/ethyl methyl carbonate (EC/EMC 3:7 by volume, Gotion) with 2% vinylene carbonate (VC, Gotion). The electrochemical characterization of the assembled cells was performed using a potentiostat (BCS-805, Bio-logic). The current density for 1C is defined as 160 mA g^{-1}. The cycling tests were performed at specified rates, ranging from 0.1 to 5C, between 3.0 and 4.3 V. The coin cell was held at 4.3 V until the current dropped below 0.05C after each charge cycle. The electrochemical impedance spectroscopy (EIS) measurements were conducted using a potentiostat (VMP-3, Bio-logic) from 10 mHz to 1 MHz, 10 mV AC signal. The cycled coin cells were discharged to 3.0 V and hold at 3 V until the current dropped below 0.0025C. All cells were rest for 12 hours before the EIS measurement.

Surface tension measurement.—The surface tension of PVDF pellets was obtained using Drop Shape Analyzer (DSA 100S, KRÜSS GmbH) at room temperature. Deionized (DI) water and DI water/ethanol 1:1 were used as the test liquids. The PVDF powders were pressed into a 12.5 mm diameter disc-shaped pellet by a pressing die at room temperature. The pressing pressure was 263 MPa.[16] The surface roughness of the pellets was measured by Optical Surface Profiler (Zygo NewView 7300). The surface energy was calculated by the Owens, Wendt, Rabel and Kaelble (OWRK) method.

Electrode porosity calculation.—The porosity of the electrode without the aluminum substrate was calculated according to the following equations:[5,32]

$$\text{Theoretical density} = \frac{1}{\left(\frac{\text{Materials wt \%}}{\text{Materials density}}\right)} \quad [1]$$

$$\text{Actual density} = \frac{\text{Electrode mass loading}}{\text{Electrode thickness}} \quad [2]$$

$$\text{Porosity} = \left(1 - \frac{(\text{Actual density})}{(\text{Theoretical density})}\right) \times 100\% \quad [3]$$

The wt% and the theoretical density of NMC and carbon black are 4.8 g cm^{-3} and 1.94 g cm^{-3}, respectively. The theoretical density of Alfa Aesar PVDF and HSV 900 PVDF are 1.76 g cm^{-3} and 1.78 g cm^{-3}, respectively.

Results and Discussion

Spray system setup.—There are two types of commercial ESD systems, turbo-charging and corona-charging. A turbo-charging system charges the sprayed particles by contacting and separating them from the wall. The charge accumulation of the particles is complex and not suitable for conductive materials. A corona-charging system charges the sprayed particles by negatively charged free ions generated from the applied electric field. A corona-charging spraying system is selected for this study because it can be utilized with both insulating and conductive materials.[33,34] For the corona-charge spraying system, the applied voltage should be high enough to charge the materials, generating enough electrostatic force to hold particles onto the substrate. However, if the applied voltage is too high, the deposited particles will quickly generate a strong electric field within the powder coating, ionizing the air trapped between powders to form positive ion and negative electron streams inside. The newly generated ion streams neutralize or oppositely charge the deposited particles, and the electron streams repel the charged particles, ejecting materials from the coating and forming surface defects.[19,35–38] Both 50 kV and 25 kV applied voltages were tested, and the coating surfaces are shown in Fig. 1. The 50 kV charged powder coating had many macroscopic defects on the surface which exposed the metal substrate underneath, shown

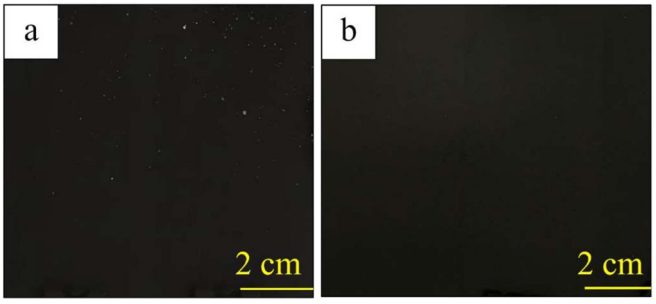

Figure 1. Photos of the surface of the electrodes made by ESD using (a) 50 kV and (b) 25 kV. The white spots are defects which expose the Al foil.

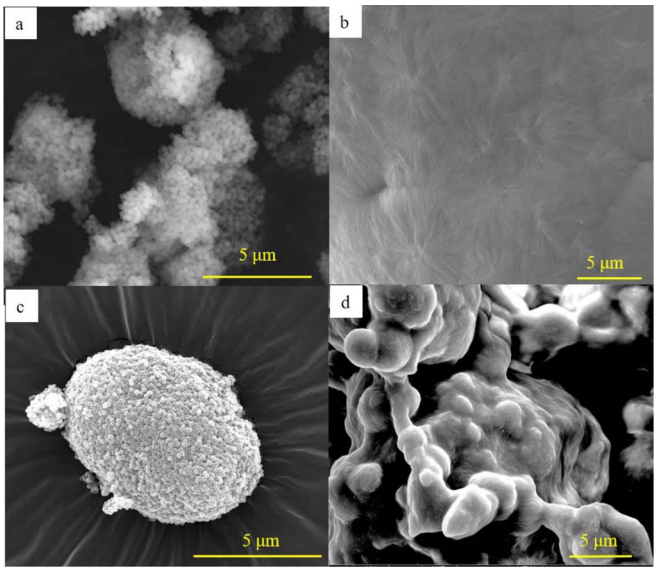

Figure 2. SEM images of PVDF powders before and after the thermal activation process: (a) and (b) are the Alfa Aesar; (c) and (d) are the HSV 900.

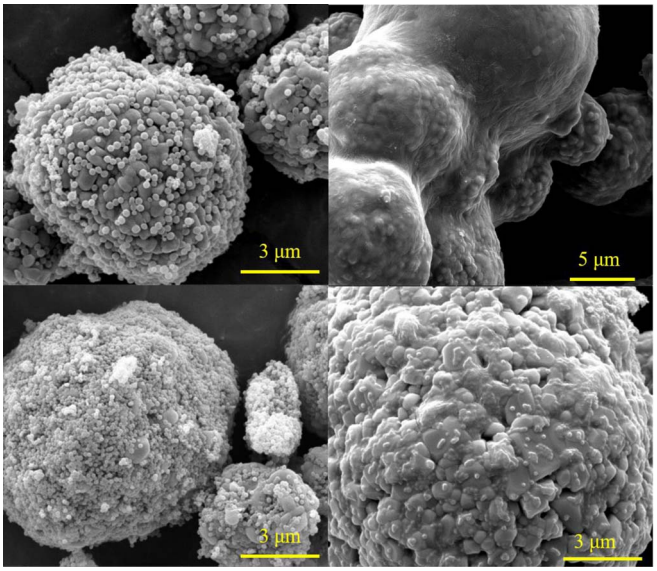

Figure 4. SEM images of: (a) NMC/Alfa Aesar before thermal activation; (b) NMC/Afla Aesar after thermal activation; (c) NMC/HSV 900 before thermal activation; (d) NMC/HSV 900 after thermal activation.

in Fig. 1a. Macroscopic defects were not observed on the surface of the 25 kV charged powder coating, shown in Fig. 1b. Therefore, the 25 kV setting was used for making the samples for testing. More images of the coating surfaces are shown in Fig. S2 in the supplementary information.

Characterization of PVDF.—To help understand the influence of the heating process, the PVDF powders were sprayed onto an aluminum substrate by the same ESD process. Afterward, the structures of PVDF particles before and after heat-treatment were investigated by SEM. As shown in Fig. 2, the as-received PVDF particles of 2 to 60 µm diameter are made of primary particles of about 300 nm diameter. After being heated at 200°C for 1 hour, the Alfa Aesar PVDF completely covered the substrate, while the primary HSV900 PVDF particles grew larger but still retained their spherical shape.

The flow behavior of polymer melt under zero pressure is mainly influenced by molecular weight distribution and heating time.[39–41] Also, the melt flow behavior may be affected by surface tension, caused by different additives. The surface tension of the PVDF pellets was measured to investigate possible surface tension effect.[16] The contact angles of DI water droplets on Alfa Aesar and HSV 900 pellets were 86.74° and 87.25°, respectively. The contact angles of DI water/ethanol 1:1 droplet on Alfa Aesar and HSV 900 pellets were 37.00° and 36.63°, respectively. The surface tensions measured by Sessile Drop Technique were 24.37 mN m^{-1} (Alfa Aesar PVDF) and 25.03 mN m^{-1} (HSV 900 PVDF), showing that the surface tension of these two polymers is very similar. The small surface tension difference may come from the surface roughness, which is 0.299 ± 0.013 µm for Alfa Aesar pellet and 0.255 ± 0.003 µm for HSV 900 pellet.[42] The typical surface maps are shown in Fig. S3 in the supplementary information.

The HSV 900 PVDF particles were baked at 200°C for up to 5 hours to investigate the influence of heating time on the flow behavior of HSV 900, shown in Fig. 3. The HSV 900 PVDF particles retain their spherical shape without spreading on the substrate, showing that the limited melt flow behavior of HSV 900 PVDF blends at 200°C is mainly caused by its high molecular weight.[41,43]

Characterization of electrode structure.—The PVDF powders were mixed with NMC particles to study the wettability of PVDF on the NMC surfaces, shown in Fig. 4. The weight ratio (NMC: PVDF) was 18:1. The secondary PVDF particles broke during the dry mixing process, forming a thin layer on the NMC surface. After the thermal activation process, the molten Alfa Aesar PVDF particles covered the NMC surface completely, forming a dense layer. In contrast, the molten HSV 900 PVDF partially covered the NMC surface.

The morphology of the thermal activated NMC/CB/PVDF powder mixture is shown in Figs. 5a–5e. In the powder mixture with Alfa Aesar, a thin PVDF layer is found on the NMC surface, shown in Figs. 5b–5c. This structure is consistent with the observation in Fig. 4b. The added CB particles were bound to the NMC surface by the molten PVDF. In the powder mixtures with HSV 900 PVDF, a porous layer was found on the NMC surface, shown in Fig. 5e. This can be understood as that the high molecular weight of HSV 900 PVDF can restrain the polymer from flowing freely on the NMC surface during the thermal activation process. As a result, they only bound the CB or PVDF particles nearby without spreading and covering the NMC

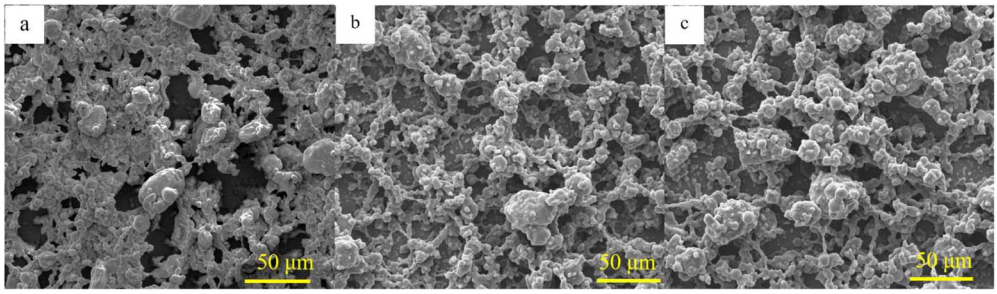

Figure 3. HSV 900 powder coating after the thermal activation process at 200°C for (a) 1 hour, (b) 2 hours, and (c) 5 hours.

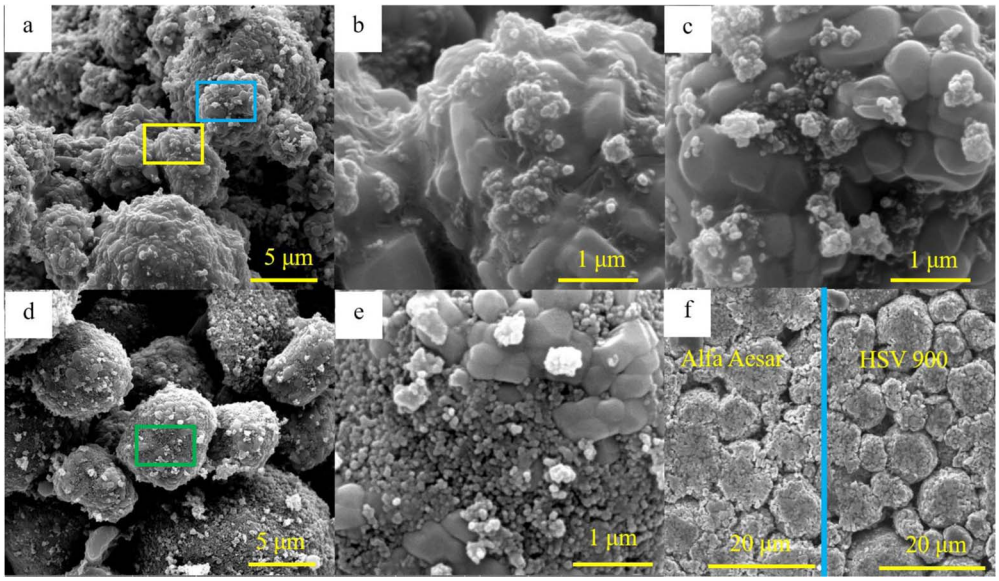

Figure 5. SEM images of NMC, CB and PVDF after thermal activation. (a) The electrode surface with Alfa Aesar PVDF. (b) and (c) The regions in yellow and blue rectangles, respectively. (d) The electrode surface with HSV 900 PVDF. (e) The region in green rectangles. (f) The electrode surfaces after calendering with Alfa Aesar PVDF (left) and HSV900 PVDF (right).

particles completely. Some bare NMC areas and CB/PVDF aggregations were observed in both the electrode powders. The broken NMC particles were found on both electrode surfaces after calendering.

Characterization of binding strength.—The binding strengths of the electrodes were measured by 180° peel test based on the ASTM D903 standard.[44] The measured peel strengths are shown in Fig. 6a. The dry-powder-coated electrode with Alfa Aesar PVDF has a slightly higher average peel strength (0.04 N cm^{-1}) than the electrode with HSV 900 (0.03 N cm^{-1}), which may be caused by the increased interface between molten PVDF and Al substrate. The substrate surfaces after peel test are shown in Figs. 6b–6d. The electrode substrate with Alfa Aesar PVDF had some NMC particles left on the surface, showing the failure occurred both within the electrode and at the electrode – substrate interface, and both PVDF/NMC cohesion and PVDF/Al adhesion contribute to the measured peel strength. The electrode substrate with HSV 900 PVDF had barely any NMC particles left on the surface, showing that the failure occurred mainly at the electrode – substrate interface. Therefore, the HSV 900 samples have smaller variations in peel strength than the Alfa Aesar samples.

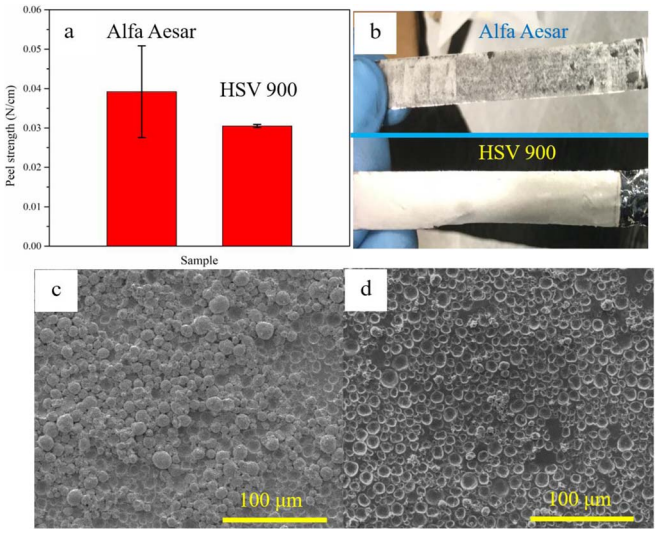

Figure 6. (a) Binding strength of the dry-powder-coated strips. (b) Sample substrates after the peel test. (c) and (d) SEM images of sample substrate surface after peel tests.

To further investigate the cohesive strength of the dry-powder-coated electrode particles, a scratch test was carried out. The friction force was measured along a 2000 µm long track, shown in Fig. 7. Two typical scratch plots were selected as examples to show the trends in Fig. 7a. According to Chen et al., the cohesive strength between particles is related to the ratio of the friction force and applied force.[45] As shown in Fig. 7b, under the same applied loads, the measured friction force traces overlap, indicating the cohesion provided by these two PVDFs is very similar.

To have a better understanding of the binding mechanism in dry-powder-coated electrodes, the cross-section structure with EDS mapping of a dry-powder-coated electrode was investigated, shown in Fig. S4 in the supplementary information. The thermal activated PVDF polymer binds the electrode particles and current collector through the van der Walls interactions, which is the same as electrodes made by the wet-slurry-coated process.[26,46] Although the molten PVDF with lower molecular weight spreads and covers more area of NMC particles, only the PVDF in between the necking region connecting two neighboring NMC particles can provide the binding force, which is consistent with the results of Ludwig et al.[16] Therefore, the PVDF layers formed on the NMC surface have a limited contribution to improving the binding strength.

Characterization of electrochemical performance.—The electrochemical properties of the dry-powder-coated electrodes were tested in the coin cell figuration. The cell information details are shown in Table II.

The cycling performance of the dry-powder-coated electrodes is shown in Fig. 8a. Although the peel strength of the electrode made with HSV 900 is slightly lower than the one made with Alfa Aesar, the performance of the electrode was not affected. The electrodes were cycled at 0.2C for the 3 cycles and then at 0.5C for 47 cycles. The specific discharge capacity of the dry-coated electrodes made with Alfa Aesar PVDF (Alfa_dry) and HSV 900 PVDF (HSV_dry) are 159 and 161 mAh g^{-1} at 0.2C and are 153 and 155 mAh g^{-1} at 0.5C, respectively. After the 50 cycles, the capacities were 148 and 146 mAh g^{-1}. Overall, the electrochemical performance of the dry-powder-coated electrodes with different PVDF binders are

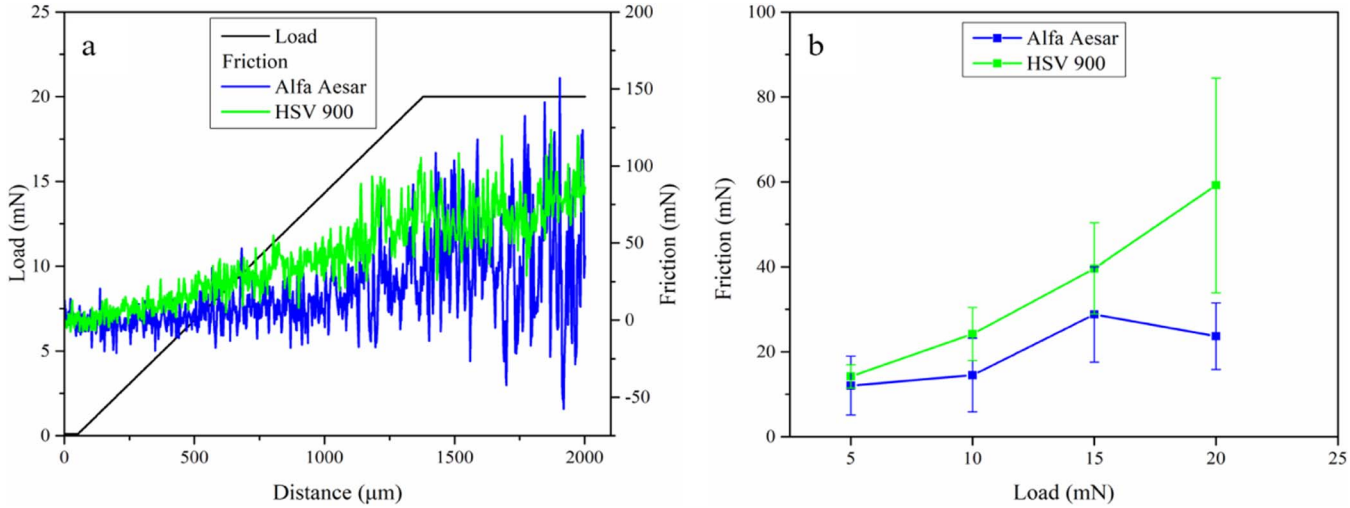

Figure 7. The scratch test of dry-powder-coated electrodes. (a) Plots of applied load and friction force as a function of scratch distance. (b) Plots of friction force as a function of applied load.

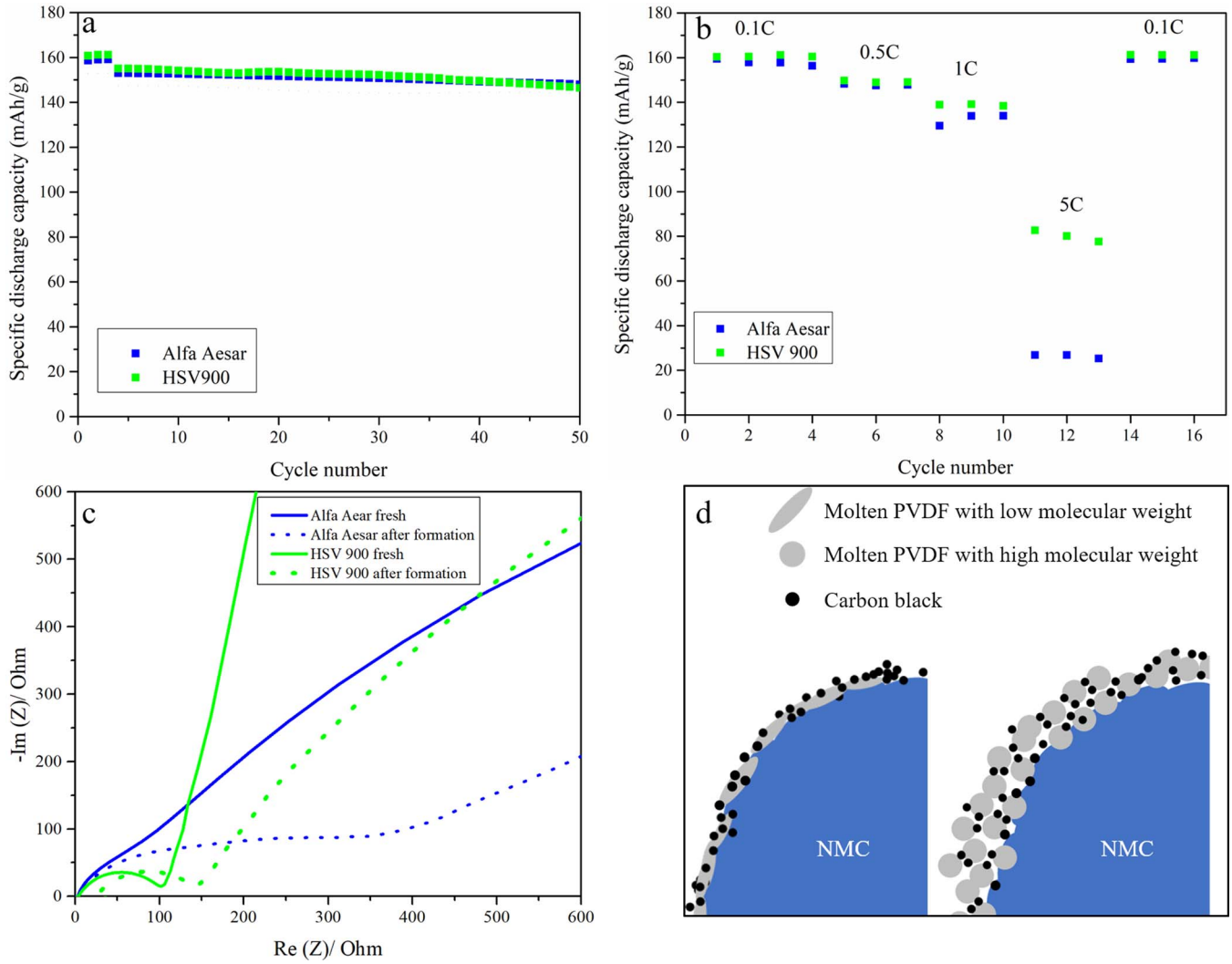

Figure 8. Electrochemical measurement results (a) long-term cycling performance; (b) C-rate performance; (c) EIS of dry-powder-coated electrodes. (d) The schematic illustration of NMC surfaces with different PVDFs after thermal activation.

Table II. Coin cell information.

Test	Electrode mass (mg cm^{-2})	Thickness (μm)	Porosity (%)
	Alfa_dry		
long term cycling	16.9	59.0	31
C-rate cycling	16.7	58.7	32
	HSV_dry		
long term cycling	17.0	59.0	31
C-rate cycling	16.8	59.3	31

similar. After the 50th cycle, the capacity retentions of Alfa_dry and HSV_dry were 93% and 91%, respectively.

The C-rate performance is shown in Fig. 8b. The specific discharge capacity of Alfa_dry was 159, 148, 133, and 27 mAh g^{-1} at 0.1, 0.5, 1, and 5C, respectively. The specific discharge capacity HSV_dry was 160, 150, 139, and 82 mAh g^{-1} at 0.1, 0.5, 1 and 5C, respectively. The specific discharge capacities were similar for both dry-powder-coated electrode at low C-rate from 0.1C to 0.5C. At 1C and 5C, the capacity of Alfa_dry decreased more significantly than HSV_900. The capacity of Alfa_dry was 16.7% of its initial capacity at 5C, while HSV_dry retained 50% of its initial capacity. The electrochemical performance of the electrodes made by a conventional wet-slurry-coating process is shown in Fig. S5 in the supplementary information.

The electrochemical impedance spectroscopy (EIS) was performed to help understand the rate capability difference.[47,48] The Nyquist plot usually consists of a semicircle at high frequency and a Warburg tail at low frequency, representing the interfacial impedance and diffusion-resistance from the electrode material, respectively. The Nyquist plots of the coin cells after assembly and formation cycles are shown in Fig. 8c. The plots of Alfa_dry have larger semicircle radius, indicating that it had very high interfacial resistance and lower rate capability than HSV_dry. The electrochemical performance difference may be explained as follows: The NMC particles in the dry-powder-coated electrodes are partially covered by the PVDF/CB agglomerations after ESD process. During the thermal activation process, the molten PVDF agglomerations bond the neighboring NMC particles, and the rest of the agglomerations form a thin layer on the NMC particles. The schematic illustrations of the NMC surfaces made with different PVDFs are shown in Fig. 8d. After the thermal activation, the PVDF with low molecular weight spreads more evenly on the NMC surface, forming a dense layer. This layer blocks the lithium ion transport, increasing the interfacial resistance of the electrode. For the PVDF with high molecular weight, the layer is porous. The electrode with this porous layer has a lower interfacial resistance because the electrolyte can fill the pores, enhancing the high C-rate performance.

Conclusions

The effects of PVDF molecular weight on NMC electrodes made by dry-powder-coating were studied. The results show that a thin layer of PVDF formed on the NMC surface after the thermal activation process, acting as binding points and lithium intercalation/deintercalation barriers. By increasing the molecular weight of the PVDF, the layer became more porous, and capacity retention was improved from 17% to 50% without decreasing the binding strength and long-term cycling performance. Thus, PVDF with high molecular weight is preferable for the electrode made by the dry-powder-coating process. Whereas the molecular weight of PVDF used in the wet-slurry-coating process needs to be controlled to meet the requirement of casting viscosity; the dry-powder-coating process may allow even higher molecular weight PVDFs to be used which may help improve bonding strength. Future work will focus on the improvement of the binding strength of the electrode, and the study of the high C-rate performance by incorporating higher molecular weight PVDFs.

Acknowledgments

We would like to thank Dr. Steven Baxter, Dr. Ramin Amin-Sanayei, and Dr. Wensheng He of Arkema Inc. for helpful discussions and for providing some of the PVDF materials used in this work. We would thank Adam Price of Unviersity of Kentucky for helping with the surface roughness measurement. We would also thank Mohammad Saiful Islam and Nicholas Cprek of University of Kentucky and two visiting students, Dawei Li from Shanghai University and Vincent Kelly from Kentucky State University, for technical assistance. This work was supported by the National Science Foundation Award 1355438 "Powering the Kentucky Bioeconomy for a Sustainable Future."

ORCID

Ming Wang https://orcid.org/0000-0001-9661-2180
Jiazhi Hu https://orcid.org/0000-0001-9102-9252
Yikai Wang https://orcid.org/0000-0002-1156-0324
Yang-Tse Cheng https://orcid.org/0000-0003-0737-9212

References

1. J. M. Tarascon and M. Armand, *Nature*, **414**, 359 (2001).
2. G.-A. Nazri and G. Pistoia, *Lithium batteries: science and technology*, Springer Science & Business Media (2008).
3. J. Li, Z. Du, R. E. Ruther, S. J. AN, L. A. David, K. Hays, M. Wood, N. D. Phillip, Y. Sheng, C. Mao, S. Kalnaus, C. Daniel, and D. L. Wood, *JOM*, **69**(9), 1484 (2017).
4. Q. Wu, S. Ha, J. Prakash, D. W. Dees, and W. Lu, *Electrochimica Acta*, **114**, 1 (2013).
5. T. Marks, S. Trussler, A. Smith, D. Xiong, and J. Dahn, *Journal of The Electrochemical Society*, **158**(1), A51 (2011).
6. G. Berckmans, M. Messagie, J. Smekens, N. Omar, L. Vanhaverbeke, and J. Van Mierlo, *Energies*, **10**(9), 1314 (2017).
7. N. Wang, Y. NuLi, S. Su, J. Yang, and J. Wang, *Journal of Power Sources*, **341**, 219 (2017).
8. Future Market Insights, N-Methyl-2-Pyrrolidone (NMP) Market: Improved Safety to Become Top Priority in Various Application Areas: Global Industry Analysis 2013 - 2017 and Opportunity Assessment 2018 - 2028 (2018).
9. A. Hunt and N. Dale, Economic valuation in 1-Methyl-2-pyrrolidone (NMP), OECD Publishing (2018).
10. U. S. Environmental Protection Agency, Fact Sheet: N-Methylpyrrolidone (NMP) (2015).
11. B. Åkesson, *World Health Organization, Geneva*, Concise International Chemical Assessment Document 35 N-Methyl-2-Pyrrolidone (2001).
12. Z. Du, K. M. Rollag, J. Li, S. J. An, M. Wood, Y. Sheng, P. P. Mukherjee, C. Daniel, and D. L. Wood, *Journal of Power Sources*, **354**, 200 (2017).
13. N. Loeffler, J. von Zamory, N. Laszczynski, I. Doberdo, G.-T. Kim, and S. Passerini, *Journal of Power Sources*, **248**, 915 (2014).
14. D. L. Wood III, J. Li, and C. Daniel, *Journal of Power Sources*, **275**, 234 (2015).
15. J. Li, B. L. Armstrong, J. Kiggans, C. Daniel, and D. L. Wood, *Journal of the Electrochemical Society*, **160**(2), A201 (2013).
16. B. Ludwig, Z. Zheng, W. Shou, Y. Wang, and H. Pan, *Sci Rep*, **6**, 23150 (2016).
17. M. Al-Shroofy, Q. Zhang, J. Xu, T. Chen, A. P. Kaur, and Y.-T. Cheng, *Journal of Power Sources*, **352**, 187 (2017).
18. M. Naito, A. Kondo, and M. Yamaguchi, *Transactions of JWRI*, **44**(2), 9 (2015).
19. D. Sauer, M. Cerea, J. DiNunzio, and J. McGinity, *International journal of pharmaceutics*, **457**(2), 488 (2013).
20. C. Zhu, Y. Fu, and Y. Yu, *Advanced Materials*, **31**(1), 1803408 (2019).
21. J. Liu, B. Ludwig, Y. Liu, Z. Zheng, F. Wang, M. Tang, J. Wang, J. Wang, H. Pan, and Y. Wang, *Advanced Materials Technologies*, **2**(10), 1700106 (2017).
22. G. Lutringer and G. Weill, *Polymer*, **32**(5), 877 (1991).
23. M. Zheng, X. Fu, W.-H. K. Zhong, Y. Wang, L. Scudiero, and J. Reeve, *ChemElectroChem*, (2018).
24. W. Bauer and D. Nötzel, *Ceramics International*, **40**(3), 4591 (2014).
25. J. C. Barbosa, J. P. Dias, S. Lanceros-Mendez, and C. M. Costa, *Membranes (Basel)*, **8**(3), (2018).
26. Y. H. Lee, J. Min, K. Lee, S. Kim, S. H. Park, and J. W. Choi, *Advanced Energy Materials*, **7**(8), 1602147 (2017).
27. J. Xu, S.-L. Chou, Q.-f. Gu, H.-K. Liu, and S.-X. Dou, *Journal of Power Sources*, **225**, 172 (2013).
28. T. L. Silva, S. Morales-Torres, J. L. Figueiredo, and A. M. Silva, *Desalination*, **357**, 233 (2015).
29. Z. Chen, D. Rana, T. Matsuura, D. Meng, and C. Q. Lan, *Chemical Engineering Journal*, **276**, 174 (2015).
30. Arkema Inc. "*Performance Characteristics & Data*" Brochure.
31. Thermo Fisher Scientific Chemicals, "*Safety Data Sheet*", Vol. 2019.
32. M. N. AL-Shroofy, Theses and Dissertations–Chemical and Materials Engineering, **76** (2017).

33. W. Kaialy, *Int J Pharm*, **503**(1−2), 262 (2016).
34. L. K. Prasad, J. W. McGinity, and R. O. Williams, 3rd, *Int J Pharm*, **505**(1−2), 289 (2016).
35. F. Wang and R. Martinuzzi, *Powder technology*, **150**(1), 20 (2005).
36. S. Guskov, Vol. 2019. Nordson Corporation (2017).
37. L. K. Prasad, J. W. McGinity, and R. O. Williams III, *International journal of pharmaceutics*, **505**(1−2), 289 (2016).
38. M. Barletta, A. Gisario, G. Rubino, and V. Tagliaferri, *Surface and Coatings Technology*, **201**(6), 3212 (2006).
39. Z. Tadmor and C. G. Gogos, *Principles of polymer processing*, John Wiley & Sons (2013).
40. M. Kaseem, K. Hamad, H. W. Yang, Y. H. Lee, F. Deri, and Y. G. Ko, *Polymer Science Series A*, **57**(2), 233 (2015).
41. J. C. Haley and T. P. Lodge, *Journal of Rheology*, **48**(2), 463 (2004).
42. A. Davoodabadi, J. Li, Y. Liang, R. Wang, H. Zhou, D. L. Wood, T. J. Singler, and C. Jin, *Journal of The Electrochemical Society*, **165**(11), A2493 (2018).
43. E. M. Friedman and R. S. Porter, *Transactions of the Society of Rheology*, **19**(4), 493 (1975).
44. ASTM International, *D903-98(2017) Standard Test Method for Peel or Stripping Strength of Adhesive Bonds.*
45. J. Chen, J. Liu, Y. Qi, T. Sun, and X. Li, *Journal of The Electrochemical Society*, **160**(9), A1502 (2013).
46. K. J. Bigham, *Zeus Industrial Products Technical Paper*, Drawn Fiber Polymers: Chemical and Mechanical Features (2018).
47. V. Ovejas and A. Cuadras, *Batteries*, **4**(3), 43 (2018).
48. S. S. Zhang, K. Xu, and T. R. Jow, *Electrochimica Acta*, **49**(7), 1057 (2004).